Liquefaction flow failure evaluation of earth dams

Evaluation de la liquéfaction des barrages en terre

R. MOHAMAD, Graduate Student, Department of Civil Engineering, Rensselaer Polytechnic Institute, Troy, NY, USA
P. DAKOULAS, Graduate Student, Department of Civil Engineering, Rensselaer Polytechnic Institute, Troy, NY, USA
G. GAZETAS, Associate Professor of Civil Engineering, Rensselaer Polytechnic Institute, Troy, NY, USA
R. DOBRY, Professor of Civil Engineering, Rensselaer Polytechnic Institute, Troy, NY, USA

SYNOPSIS A new approach for liquefaction flow failure evaluation of earth dams is presented. The method applies steady-state concepts, and is based on the premise that flow failure of an earth dam takes place in two consecutive stages: a first stage of pore pressure buildup, controlled by the horizontal seismic shear strains, γ_c, and a second stage of unidirectional steady-state flow failure, driven by the static shear stresses, τ_s, associated with the weight of the sliding mass. A simplified method of determining γ_c is also presented.

INTRODUCTION

Seismic shaking of earth dams and embankments comprising zones of, or founded on, saturated cohesionless sands or silts can build up pore pressures in these materials, with the possible development of liquefaction flow slides. A number of such flow slides have been reported in the literature (e.g. Dobry and Alvarez, 1967; Seed, 1979; Ishihara et al., 1978).

PROPOSED METHOD

In this paper, a new method for the liquefaction flow failure evaluation of earth dams and embankments is proposed. This new approach differs significantly from the Seed-Lee-Idriss (see Seed, 1979) procedure in the following fundamental aspects:(i) it applies steady-state concepts for the flow failure as developed by Castro and his co-workers (Castro, 1975; Castro and Poulos, 1977; GEI, 1982); (ii) it recognizes that cylic shear strain is the fundamental parameter controlling pore pressure buildup during seismic loading (Dobry et al., 1982); (iii) it is based on the central concept that there are two different consecutive stages in the flow failure of an earth dam: a first stage of pore pressure buildup, mainly controlled by the level of seismic (cyclic) shear strains, γ_c, and a second flow failure stage driven by the static shear stresses, τ_s, associated with the weight of the dam; and (iv) it recognizes that γ_c and τ_s in the field generally act on different planes, and simulates this fact in the laboratory with a new testing procedure, which is designated as strain-controlled CyT-$\overline{\text{CAU}}$ test, and is described below.

A NEW LABORATORY TESTING PROCEDURE

The authors have developed a new type of axial/torsional test to simulate more realistically the two stages of field liquefaction flow failure. In this strain-controlled CyT-$\overline{\text{CAU}}$ test (see Fig. 1) the simulated static shear stress before the earthquake is applied on a 45° plane by anisotropically consolidating the specimen under stresses $\bar{\sigma}_{10}$ and $\bar{\sigma}_{30}$, such that $K_c=\bar{\sigma}_{10}/\bar{\sigma}_{30} > 1$. The maximum static shear stress is then $\tau_s = (\bar{\sigma}_{10}-\bar{\sigma}_{30})/2$. Next, a torsional horizontal cyclic shear strain, γ_c, simulating the seismic action, is applied in undrained condition, and a pore pressure buildup is induced (first stage defined above). If the specimen is contractive, and if τ_s is greater than the steady-state or residual shear strength of the specimen, S_{us}, flow failure is triggered after a certain number of cycles (second stage).

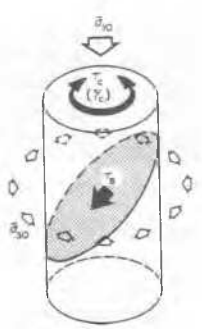

Fig. 1 Applied Stresses in a CyT-$\overline{\text{CAU}}$ Test
$[\tau_s= (\bar{\sigma}_{10}-\bar{\sigma}_{30})/2;\ K_c = \bar{\sigma}_{10}/\bar{\sigma}_{30}]$

Results of a typical CyT-$\overline{\text{CAU}}$ test are shown in Fig. 2. During horizontal cyclic straining, the static shear stress on the 45° plane, $\tau_s = q_s$, remains unchanged, while the pore pressure is building up. Then, at point T, unidirectional flow deformation is triggered. Point T in this case was reached after 15 cycles, whereas the flow failure stage after T took only 0.7 sec. In this as well as other tests the flow failure is driven by the axial (deviatoric) load, not by the torsional load. The stress conditions represented by points S in the figure correspond to

the steady-state condition for the specimen where the steady-state shear stress, S_{us}, and effective normal stress, $\bar{\sigma}_{3us}$, are unique functions of the void ratio, e, of the sand (the subscript 'us' denotes 'undrained steady-state'). By performing several tests on the same sand at different void ratios, e vs S_{us} and e vs $\bar{\sigma}_{3us}$ steady-state lines for the particular sand can be obtained. The ratio $\tan \bar{\alpha}_{us} = S_{us}/\bar{p}_{us}$ [see Fig. 2c] defines the steady-state or residual strength envelope for the sand, which is independent of void ratio. Furthermore, the steady-state lines and $\bar{\alpha}_{us}$ are the same whether obtained from CyT-$\overline{CAU}$ tests,

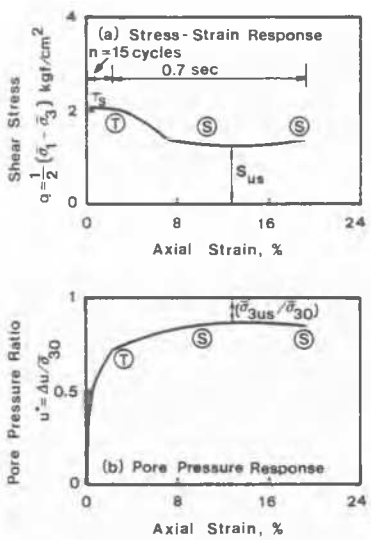

Fig. 2 Typical Results of a CyT-$\overline{CAU}$ Test on a Contractive Specimen of Banding Sand [e=0.781; Relative Density, D_r = 23%; $\bar{\sigma}_{30}$ = 8.3 kgf/cm²; Kc=1.5; Peripheral Cyclic Shear Strain = 0.29%]

monotonic $\overline{CIU}$ or $\overline{CAU}$, or from cyclic $\overline{CAU}$ tests (See GEI, 1982; Dobry et al., 1984; Mohamad and Dobry, 1984).

An important finding based on a number of CyT-$\overline{CAU}$ tests performed by the authors on Banding sand is that flow failure is always triggered when the effective stress path reaches the steady-state or residual strength envelope, $\bar{\alpha}_{us}$ (Dobry et al., 1984). This is illustrated in Fig.(2c). This means that points T and S lie on the same $\bar{\alpha}_{us}$ envelope. Thus, for a given K_c and $\bar{\alpha}_{us}$, the pore pressure ratio, $u^*_T = \Delta u_T/\bar{\sigma}_{30}$ which must be developed in a contractive specimen in order to reach the $\bar{\alpha}_{us}$ envelope and trigger the flow failure, is given by:

$$u^*_T = [K_c + 1 - (K_c - 1)/\tan \bar{\alpha}_{us}]/2 \qquad (1)$$

OUTLINE OF NEW APPROACH

The main steps of the proposed method are:

(1) Determine the static principal effective stresses, $\bar{\sigma}_1$ and $\bar{\sigma}_3$ throughout the dam and its foundation, before the earthquake by using FE analysis techniques.

(2) Determine the e vs $\bar{\sigma}_{3us}$ and e vs S_{us} steady-state lines for the sands in the dam, by running CyT-$\overline{CAU}$ tests, or monotonic $\overline{CIU}$ or $\overline{CAU}$ tests, combined with field measurements or other means of estimating in-situ void ratios. This may require the laboratory testing program to include tests on both remolded and undisturbed specimens (GEI, 1982.) Also, from the same tests, determine $\bar{\alpha}_{us}$, the steady-state strength envelope angle.

(3) Determine within the dam and its foundation the zone(s) of contractive, saturated sand, where $\bar{\sigma}_3 > \bar{\sigma}_{3us}$ (Fig. 3).

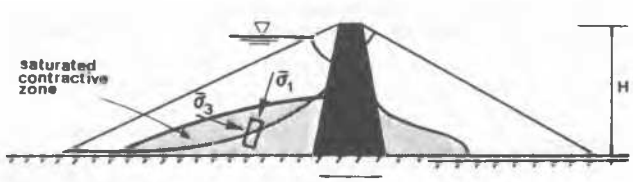

Fig 3. Sketch of Earth Dam Showing Contractive Zone and Potential Slide Surface

(4) Perform a static slope stability analysis of the dam, using values of S_{us} obtained from step (3) as the shear strength of the contractive zone(s). This is conservative, and assumes that for the whole contractive zone(s) the pore pressures and strains caused by the seismic shaking are large enough to drop the shear strength to the value S_{us}.

(5) If the slope stability analysis in (4) indicates that the dam may be unsafe, the next step is to determine the actual magnitude and duration in cycles, n, of the equivalent uniform cyclic shear strains, $\gamma_c = \delta\gamma_{max}$, induced by the design earthquake (δ<1). If most of the sand within the dam is subjected to $\gamma_c < \gamma_t$, where γ_t is the threshold cyclic shear strain below which there is no pore pressure buildup (Dobry et al., 1982; Dyvik et al., 1982), the evaluation ends here, and the dam can be considered safe for the given earthquake. The value of the threshold strain, γ_t, has been shown to be insensitive to anisotropic consolidation (Dyvik et al., 1982), and for most clean quartz sands, it is $\gamma_t \approx 10^{-2}$% (Dobry et al., 1982).

(6) If a significant portion of the cohesionless soil in the dam experiences $\gamma_c=\delta\gamma_{max} > \gamma_t$, a detailed investigation is necessary. This may include refining the calculation of γ_c by dynamic FE analyses, and conducting a series of CyT-$\overline{CAU}$ tests on soil specimens with void ratios and consolidation effective stresses covering the range within the dam. For a soil element in a contractive zone within the dam, the value of u^* (γ_c,n,D_r,K_c) at successive times during the earthquake, where u^* is obtained from the CyT-$\overline{CAU}$ tests, must be compared with u^*_T for the element. When $u^*=u^*_T$, the soil element is assigned a shear strength equal to S_{us}. A static slope stability analysis is conducted to evaluate the danger of flow failure at the end of the shaking, and can also be performed at

different times during the earthquake. A factor of safety of 1 or less in this static analysis predicts flow failure of the dam.

SIMPLIFIED ANALYSIS FOR SESMIC SHEAR STRAINS

There are a number of analytical and FE methods to determine the cyclic shear strains, γ_c, induced by the earthquake. For the case in which the dam is founded on a stiff foundation soil which cannot liquefy, the authors have developed a simplified method based on the shear beam model. In this method, the dam is idealized as an infinitely long, viscoelastic, triangular wedge deforming only in shear and thus experiencing only horizontal seismic shear stresses and strains. The model assumes a uniform distribution of horizontal lateral displacements and of shear stresses and strains across the width of the dam. The inhomogeneity of the dam is accounted for by taking the shear modulus as varying with depth in the form: $G(x) = G_b (x/H)^{\mu} = G_b y^{\mu}$ where G_b is the shear modulus at the base of the dam, x = depth from the crest and μ = a constant coefficient, which, on the basis of field and analytical evidence, can be taken approximately as 2/3 (Gazetas and Abdel-Ghaffar, 1981; Gazetas, 1981). For μ = 2/3, the expression for the shear strain at the normalized depth y = x/H is:

$$\gamma(y) = -\frac{4}{3\gamma H}\sum_{j=1}^{\infty}\frac{A_j}{a_j}\{y^{-2/3}\sin[a_j(1-y)^{2/3})\} + a_j\cos[a_j(1-y^{2/3})]\}S_{dj}(t) \quad (2)$$

where the eigenvalues a_j are given by Gazetas (1982), and the modal response $S_{dj}(t)$ is evaluated numerically for the earthquake input

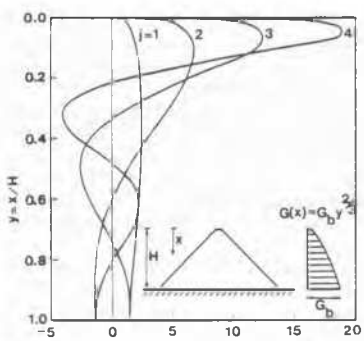

Fig. 4 Shear Strain Modal Shapes

by means of the Duhamel integral. A_j are correction factors accounting for canyon geometry; for long dams A_j=1. Fig. 4 presents the first four modes of shear strain (multiplied by the corresponding modal participation factors). To examine the distribution of maximum seismic shear strains within a dam, a series of detailed FE analyses were performed, using a number of different idealized dams subjected to four historic earthquake records. Fig. 5 presents the geometry and some of the results for two of these dams. In these analyses each element was assigned a shear modulus, G, proportional to the square root of its confining pressure by a series of iterative static FE analyses. To isolate the effect of the core,

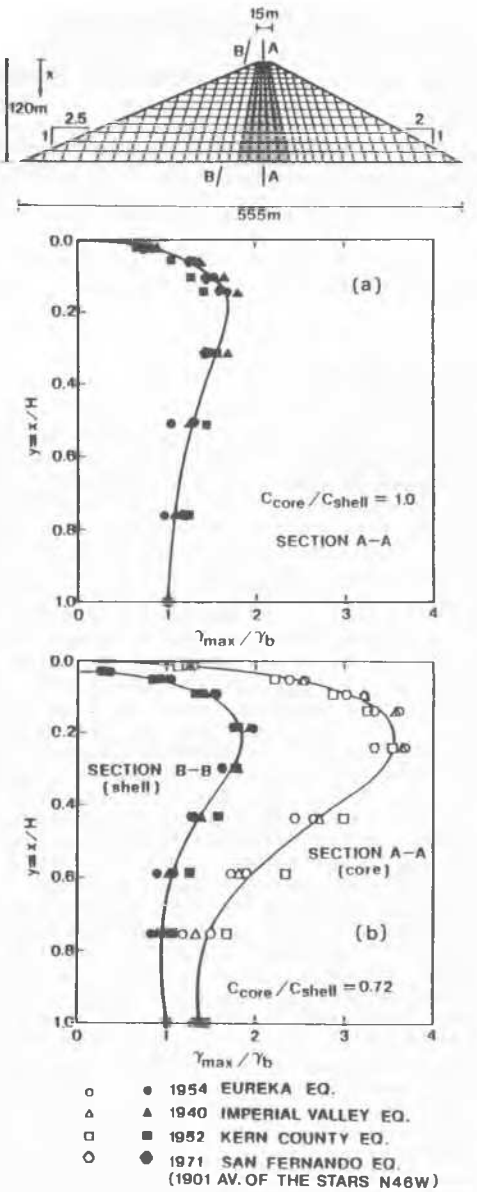

Fig. 5 Variation of Maximum Shear Strain [C_{ave}=280 m/sec; Damping β=10%]

different values of shear wave velocity ratios, C_{core}/C_{shell}, were used, corresponding to the same confining pressure. Fig. 5(a) shows the strains along the central cross-section A-A, for the case of a ratio C_{core}/C_{shell} = 1. These strains are peak values occurring at different times. Also plotted is the average curve for the four earthquake records. It has also been found that the strain is quite uniform across the width of the dam. Fig. 5(b) shows the distribution of the maximum seismic shear strain for a dam of the same geometry and the same average shear wave velocity (C=280m/ sec), but having a ratio C_{core}/C_{shell}= 0.72. In all these cases, the shear strains were normalized with respect to the strain at the shell base, γ_b. The data points in Fig.5(b) show

that the maximum shear strain in the core (section A-A) is higher than in the shell (section B-B). It is interesting to note that the distribution of maximum shear strain in the shell is similar to the distribution in Fig. 5(a). Furthermore, other results, not presented in Fig. 5(b), show that the maximum shear strain remains uniform within the shell. The maximum shear strain at the base, γ_b, can be calculated by the two-mode approximation:

$$\gamma_b = [\gamma_{b1}^2 + \gamma_{b2}^2]^{1/2} \; ; \; \gamma_{bj} = \frac{3\rho H}{G_b} \cdot \frac{A_j}{a_j^2} \cdot S_{aj} \qquad (3)$$

$$\text{where } T_j = \frac{3\pi H}{a_j} (\rho/G_b)^{1/2} \cdot B_j \qquad (4)$$

and $j = 1,2$; S_{aj} is the acceleration spectral value corresponding to the modal period T_j and the selected damping ratio; and ρ is the mass density of the soil. B_j are correction factors accounting for canyon geometry; for long dams $B_j=1$. A comparison of γ_b obtained from the same four time history analyses using the shear beam model (Eq. 2) with those estimated using Eq. 3 showed that Eq. 3 is accurate within 15% (it should be noted that Eq. (2) gives good agreement with the FE results). Once γ_b is found, the distribution of γ_{max} for the shell can be estimated with the average curve of Fig. 5(a). The use of Eq. (3) and Fig. 5(a) to estimate γ_b and γ_{max} versus x, will in general require consideration of the nonlinearity of the soil modulus G_b and damping ratio in Eqs. (3) and (4). Fortunately, both of these soil parameters change slowly with shear strain. Therefore, the variation of γ_{max} with depth in Fig. 5(a) can be neglected and an average maximum shear strain, γ_{ave}, can be selected for the whole dam. The use of this constant γ_{ave} preserves the validity of $G=G_b(x/H)^{2/3}$ and thus allows the use of the same analytical solutions, but with G_b adjusted to be consistent with γ_{ave}. Because γ_{ave} is still a peak seismic strain value, it is necessary to use the fraction $\delta\gamma_{ave}$ to enter the curves of G_b and of damping ratio versus constant cyclic shear strain. Iterations are needed to find γ_{ave}, γ_b, G_b and damping ratio in this simplified procedure, as is usually done for soils in equivalent linear response analyses. Once convergence occurs, the desired value of γ_b is obtained, and γ_{max} for different elevations within the shell is determined with the curve of Fig. 5. An approximate procedure for taking into account the effect of canyon shape on γ_b is presented elsewhere (Dobry et al., 1984; Dakoulas and Gazetas, 1984).

CONCLUSION

A new method for evaluating the safety of earth dams against earthquake-induced liquefaction flow slides has been presented. The method applies steady-state concepts, in conjunction with the cyclic shear strain approach. The method recognizes and simulates closely the fact that pore pressure buildup prior to failure is controlled by the seismic shear strains, while the flow slide itself is driven by the static shear stresses due to the weight of the sliding mass. A simplified procedure for determining the maximum seismic shear strains, using an inhomogeneous shear beam model, is also incorporated in this new method.

ACKNOWLEDGEMENTS

The authors gratefully acknowledge the assistance of Mr. Gregory E. Thomas in conducting the laboratory test illustrated by Fig. 2. This work was performed under U.S. National Science Foundation Grant No. CEE-8205345.

REFERENCES

Castro, G. (1975). Liquefaction and Cyclic Mobility of Saturated Sands. JGED, ASCE. Vol. 101, No. GT6, 551-569.

Castro, G. and Poulos, S.J. (1977). Factors Affecting Liquefaction and Cyclic Mobility. JGED, ASCE, Vol. 103, No. GT6, 501-506.

Dakoulas, P. and Gazetas, G. (1984). Seismic Response of Earth Dams in U-shaped Valleys. Submitted for publication.

Dobry, R. and Alvarez, L. (1967). Seismic Failures of Chilean Tailings Dams. JSMFD, ASCE, Vol. 93, No. SM6, 237-260.

Dobry, R., Ladd, R.S., Yokel, F.Y. and Chung, R.M. (1982). Prediction of Pore Water Pressure Buildup and Liquefaction of Sands During Earthquakes by the Cyclic Strain Method. National Bureau of Standards, U.S. Dept. of Commerce, Building Science Series 138.

Dobry, R., Mohamad, R., Dakoulas, P. and Gazetas, G. (1984). Liquefaction Evaluation of Earth Dams - A New Approach. Proc. 8WCEE, San Francisco, USA.

Dyvik, R., Dobry, R., Thomas, G.E. and Pierce, W.G. (1982). Influence of Consolidation Shear Stresses and Relative Density on Threshold Strain and Pore Pressure during Cylic Straining of Saturated Sand. Research Report No. CE-82-11, Dept. of Civil Engr., Rensselaer Polytechnic Institute, Troy, N.Y.

Gazetas, G. (1981). A New Dynamic Model for Earth Dams Evaluated through Case Histories. Soils and Foundations, Vol. 21, No. 2, 67-78.

Gazetas, G. (1982). Shear Vibrations of Vertically Inhomogeneous Dams. Int. Journal for Num. and Anal. Meth. in Geomechanics, Vol.6, No. 2, 219-241.

Gazetas, G. and Abdel-Ghaffar, A.M. (1981). Earth Dam Characteristics from Full-Scale Vibrations. Proc. 10th Int. Conf. on Soil Mech. and Fdn. Eng., Stockholm, paper 10/7, 207-210.

Geotechnical Engineers, Inc. (1982). Liquefaction Induced by Cyclic Loading. Report to Nat. Science Foundation.

Ishihara, K., Okusai, S. and Tatsuoka, F. and (1978). Slip Failures in Earth Structures Natural Slopes. Report on Damage during Izu-Oshima 1978 Earthquake, Univ. of Tokyo, 70-79

Mohamad, R. and Dobry, R. (1984). Cyclic Liquefaction Resistance of Anisotropically Consolidated Sands - A Systematic Interpretation. Research Report, Dept. of Civil Engineering, Rensselaer Polytechnic Institute, Troy, N.Y.

Seed, H.B. (1979). Considerations in the Earthquake-resistant Design of Earth and Rockfill Dams. Geotechnique, Vol. 29, No. 3, 215-263.